ADVANCED FUNCTIONAL MATERIALS
www.afm-journal.de

Breathable and Flexible Dual-Sided Nonwovens with Adjustable Infrared Optical Performances for Smart Textile

Qiang Gao, Tobias Lauster, Bernd A. F. Kopera, Markus Retsch, Seema Agarwal,* and Andreas Greiner**

Maintaining constant body temperature is the most basic function of textiles. However, traditional fabrics irradiate a massive amount of thermal energy to the ambient environment due to the high emissivity of the materials used for textiles. This phenomenon weakens the thermal function, causing vast thermal energy loss by dissipation as infrared (IR) irradiation. To improve thermal comfort and reduce extra energy consumption, smart thermal management textiles must maintain constant body temperature by regulating IR irradiation from the human body or by compensating heat losses by joule heating. Here, a smart dual-sided nonwovens' preparation procedure and properties for use as a textile with this combination of properties are shown. The nonwoven combines a high porosity with high IR reflectance and low IR emittance. The nonwoven is adjustable from reflective to emissive when turned inside out. It is consequently permeable to air and vapor and simultaneously mitigates thermal heat losses with radiation. In addition, low sheet resistance and superior flexibility make it possible to use them in flexible electronics and wearable devices. It can be further equipped with a porous Joule heating layer adding active control to the personal thermal comfort.

1. Introduction

Thousands of years ago, our ancestors used all kinds of plants to cover the body to keep it warm. In recent centuries, silk, cotton, hemp, and other natural materials were applied in the traditional textile field to realize clothing warmer and more comfortable. Textiles are revolutionized by synthetic materials such as polyesters and nylons, and incorporating smart functionalities has become a trend and research objective. The smart functionalities are introduced for monitoring body movements, detection of metabolic indexes, or energy storage.[1] For instance, solar cell integrated textile is promising for energy storage and charging portable electronic devices.[2] Initially, the textile's essential function is to keep warm and reduce body energy loss for surviving in the frigid natural environment. Traditional textiles concentrate more on lowering body heat transfer into the air surrounding via convection and conduction. However, it fails to insulate body thermal emission due to the high emissivity of ordinary cloth. If heating and insulation could be managed based on human requirements, a huge amount of energy could be saved[3] and personal thermal comfort increased. Hence, personal thermal management devices, wearable like typical textiles and capable of significantly reducing body heat loss or raising the textile temperature according to personal desire, has been developing to improve body thermal comfort control in new strategies and solutions. By regulating heat exchange (infrared (IR) radiation flow) from the human body to its surroundings, developing advanced materials with body thermal irradiation control has attracted considerable attention.[4] IR transparent radiative,[5] emissive radiative,[6] solar-reflecting radiative cooling textiles, and conductive cooling textiles with enhanced thermal conductivity[7] have been widely reported to keep cool in warm surroundings by heat exchange between human body and environment.[3] On the contrary, when in cold climate, textiles with warming purpose are highly demanded to significantly reduce heat loss into the surroundings. This is technically achieved by thermal insulating materials, such as porous aerogel fiber,[8] or IR reflecting materials via incorporating metal particles and metal wires.[6b,9] To compensate for heat dissipation through IR radiation, textiles with electro heating function are highly desired to realize

Q. Gao, S. Agarwal, A. Greiner
Department of Chemistry
Macromolecular Chemistry II and Bavarian Polymer Institute
University of Bayreuth
Universitätsstrasse 30, 95440 Bayreuth, Germany
E-mail: agarwal@uni-bayreuth.de; greiner@uni-bayreuth.de

T. Lauster, B. A. F. Kopera, M. Retsch
Department of Chemistry
Physical Chemistry I
University of Bayreuth
Universitätsstrasse 30, 95440 Bayreuth, Germany
E-mail: markus.retsch@uni-bayreuth.de

M. Retsch
Bavarian Center for Battery Technology (BayBatt)
Bavarian Polymer Institute, and Bayreuth
Center for Colloids and Interfaces
University of Bayreuth
Universitätsstrasse 30, 95440 Bayreuth, Germany

The ORCID identification number(s) for the author(s) of this article can be found under https://doi.org/10.1002/adfm.202108808.

DOI: 10.1002/adfm.202108808

the aims of harvesting energy from the human body to maintain body temperature constant, especially for those people living in harsh regions.[10]

High-performance polymers like polyimide (PI) have excellent mechanical properties, high chemical resistance and excellent thermal stability. They are often applied as filters, mechanical parts, insulation and passivation films, and medical tubing. Short electrospun fibers constructed polymeric sponge is an excellent thermal insulator with very high thermal resistance thanks to its super-high porosity.[11] Nevertheless, when some electrically conductive materials such as graphene and carbon nanotube,[12] electrically conductive polymer,[13] and metal nanowire[14] were incorporated, these polymeric materials could change their electrical property from non-conductive to conductive, even highly conductive, which often used to prepare wearable devices, such as sensor and triboelectric nanogenerator.[15] Recently, silver nanowire (AgNW) has been established as a promising electrically conductive material applied to prepare various kinds of electronic devices such as smart sensors[16] for monitoring physiological indexes, transparent touch screens,[17] and nanogenerator for energy-harvesting and storage.[18] Additionally, AgNW is also known for its ultralow IR emissivity, thanks to the low emissivity of bulk silver (≈0.02). A recently developed AgNWs coated textile showed much higher IR reflectance of ≈40% compared to uncoated textile (≈1%) and provided 21% more thermal insulation due to the reduction of radiation loss.[9] In comparison, herein, we present the preparation procedure and detailed characterization of an electrically conductive dual-sided PI/AgNW nonwoven with lightweight, highly flexible, air permeable, washable, IR-reflecting, and tailored heating properties. The IR reflecting properties are different on two different sides so that it can be used for multipurpose. The prepared PI/AgNW nonwoven is appropriate for flexible electronics and smart wearable devices and for other applications like for example sensor devices and energy devices for future use.

2. Result and Discussion

The dual-sided nonwovens were prepared, as shown in **Figure 1**. First, the PI electrospun nonwoven (thickness 48.0 ± 2.5 µm, area 10 cm^2, Figure S1a, Supporting Information) was placed on a sand core funnel, and then AgNW dispersion (different amounts of 17 g L^{-1} dispersion) was filtered through the PI nonwoven under vacuum assistance. During this process, AgNW networks were formed on top of the PI nonwoven (Figure S1b, Supporting Information). The average diameters of PI fibers and AgNWs were 0.30 ± 0.07 and 0.10 ± 0.03 µm, respectively (Figure S1c, Supporting Information). A thermoplastic polyurethane (TPU) solution was filtered through the PI/AgNW nonwoven network under light vacuum with the intention to bond AgNW networks strongly onto the PI nonwoven by residual TPU acting as glue between the two. The as-prepared nonwovens have dual sides: the AgNW network side (silver gray) and the PI nanofiber layer side (yellow) (Figure 1b). The TPU (blue regions in Figure 1c) is entangled with AgNWs and attached to the PI nonwoven, as confirmed by energy-dispersive X-ray-scanning electron microscopy (EDX-SEM) (Figure 1d). The dual-sided nonwovens are designated as PI/TPU/AgNW-X, where X denotes the volume of AgNW dispersion (17 g L^{-1}) in µL used for the preparation of nonwovens. PI/TPU/AgNW-25 and PI/TPU-AgNW-500 nonwovens have a thickness of 56.7 ± 1.0 and 57.7 ± 3.1 µm (Figure S2a, Supporting Information), respectively. The pore size (Figure 1e) of PI/TPU was centered around 1.7 µm. The dual-sided nonwoven with fewer AgNWs (PI/TPU/AgNW-25) showed a sparse AgNW network, which insignificantly affected the nonwoven's pore size (≈1.7 µm). However, the sample PI/TPU/AgNW-500 showed a decrease in pore size to 0.7 µm due to the denser layer of AgNW networks. All nonwovens were air permeable as the pore structure was retained during the preparation process using a light vacuum for the filtration of TPU and AgNWs (Figure 1f). PI/TPU, PI/TPU/AgNW-25 and PI/TPU/AgNW-500 showed air permeability of 5.2 ± 0.5, 4.3 ± 0.6, and 2.7 ± 0.6 mm s^{-1} respectively, whereas pure PI nonwoven has a permeability of 20.3 ± 0.5 mm s^{-1}. The nonwovens also presented good moisture permeability (Figure S2b, Supporting Information) (≈65 mg cm^{-2} day^{-1} for PI/TPU/AgNW-500), which is close to the value of pure PI electrospun nonwoven (≈82 mg cm^{-2} day^{-1}). Both sides of the PI nonwovens were hydrophobic with high contact angles (≈140 °, Figure S2c, Supporting Information). Although pure AgNWs are very hydrophilic, the AgNW network side of dual-sided nonwovens also showed very high contact angles (145.5 ± 0.1 and 144.9±0.5 degrees for PI/TPU/AgNW-25 and PI/TPU/AgNW-500, respectively) due to the homogeneously dispersed TPU in the network (Figure S3, Supporting Information). The dual-sided nonwovens were as strong as the pristine PI nonwoven (18 MPa in tensile strength, 77% in strain) without any significant effect of TPU or AgNWs (Figure 1g).

As both PI nonwoven and TPU are electrically insulating materials, the electrical property of the dual-sided nonwoven is significantly influenced by the amount of AgNW due to the low resistivity (1.6×10^{-8} Ω m) of silver. The polymeric nonwovens (PI and PI/TPU) showed very high electrical resistance (sheet resistance: $>10^8$ Ω sq^{-1}). The sheet resistance of the dual-sided nonwovens could be tuned to as low as 0.2 Ω sq^{-1} using appropriate amounts of AgNWs. The resistance decreased with the increasing quantity of AgNW (**Figure 2**a and Table S1, Supporting Information) with a discontinuous jump between PI/TPU/AgNW-2.5 and PI/TPU/AgNW-5 from ≈5×10^8 to ≈10^5 Ω sq^{-1}. Denser AgNW networks resulting from more AgNWs, as demonstrated by SEM images (Figure S6, Supporting Information), contributed to high conductivity, resulting in decreased sheet resistance.

The nonwovens are mechanically flexible. In the circuit with PI/TPU/AgNW-500, there was insignificant variation in luminance of the lightening light-emitting diode (LED) bulb with the nonwoven undergoing bending and twisting deformations (Figure 2b) compared to that of the virgin state. These types of bending and twisting deformations are often faced by wearable, flexible devices in everyday life. Additionally, the PI/TPU/AgNW-500 exhibited outstanding electromechanical properties. In particular, the electrical resistance shows a negligible variation (R/R_0 = 1, R and R_0 denoting resistance after and before test respectively) even after 100-time repeatable bending (bending angle: ≈140°) (Figure 2c and Figure S7, Supporting Information), indicating high durability and cyclability to withstand non-tensile deformation. When the sample was stretched to about 65% (Figure 2d), there was only a small increase in the resistance of PI/TPU/AgNW-500 from 2 to 40 Ω. In contrast, a higher resistance change was observed for dual-sided

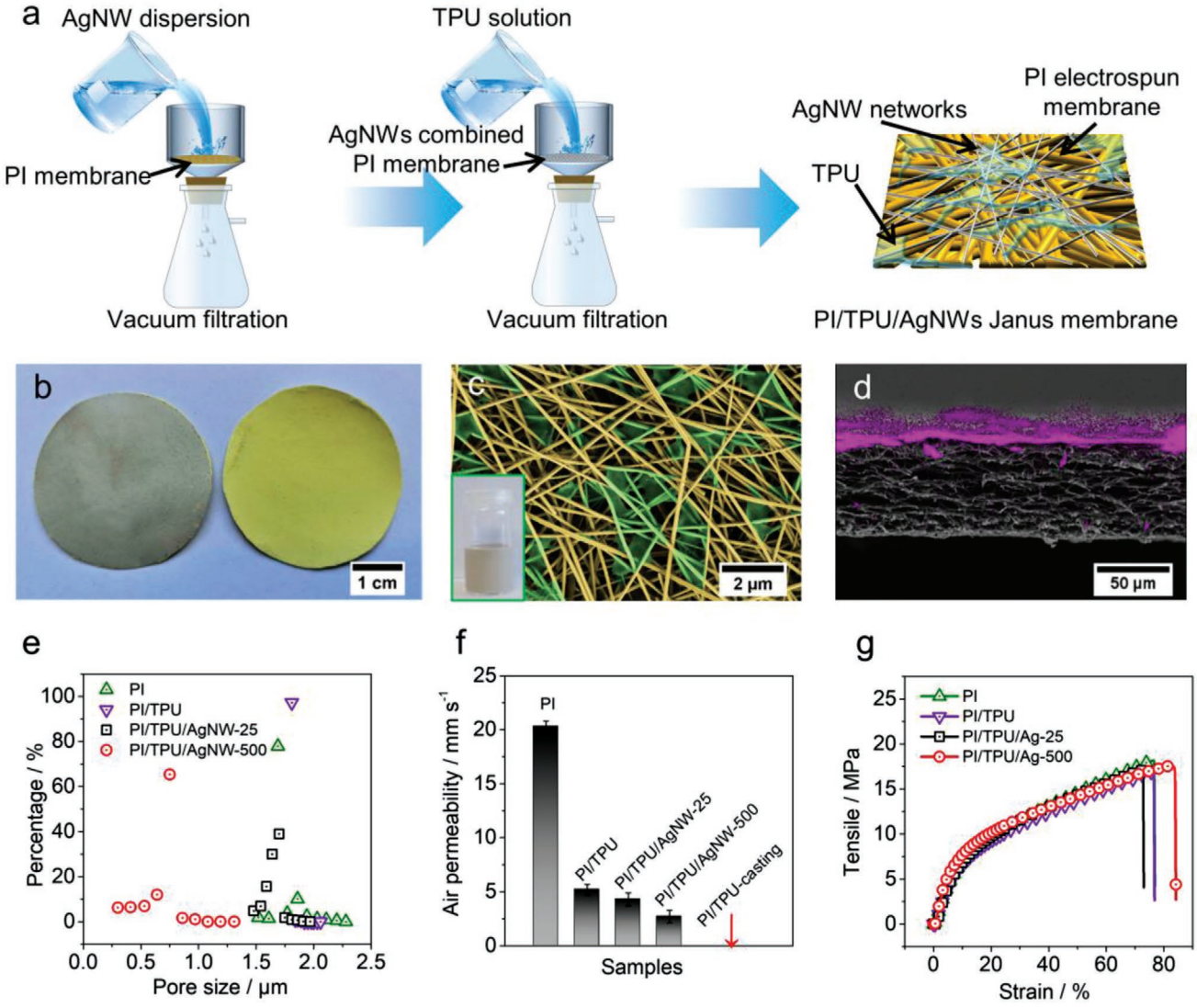

Figure 1. Preparation route a) and b) digital photographs of the dual-sided nonwoven (sliver gray: AgNW networks side, yellow: PI side). c) Photoshop colored SEM image (original image seen in Figure S4, Supporting Information) of AgNW networks with TPU:TPU colored in green. The digital photograph of the AgNW water suspension is shown in the green frame at the left corner. d) EDX-SEM image of the dual-sided nonwoven PI/TPU/AgNW-500. The purple area presented the AgNW networks. e) Pore size distributions of PI electrospun nonwoven, PI electrospun nonwoven with TPU, PI/TPU/AgNW-25, and PI/TPU/AgNW-500. f) Air permeability of PI electrospun nonwoven, PI electrospun nonwoven with TPU, PI/TPU/AgNW-25, PI/TPU/AgNW-500, and PI/TPU-casting. The sample PI/TPU-casting is prepared by casting 2 mL 8 wt% TPU solution on PI electrospun nonwoven (SEM image in Figure S5, Supporting Information). g) Mechanical properties of PI electrospun nonwoven, PI electrospun nonwoven with TPU, PI/TPU/AgNW-25, and PI/TPU/AgNW-500.

nonwovens with fewer AgNWs (PI/TPU/AgNW-25) under similar conditions. It showed a change from ≈700 to ≈8000 Ω merely within 10% strain deformation. In PI/TPU/AgNW-25 with fewer AgNWs, stretching just over 10% leads to a break in electrical percolation due to the fracture of AgNW networks leading to the loss of conductivity. The dense network of AgNWs in PI/TPU/AgNW-500 is responsible for tolerating a large deformation without losing performance, despite the network fractures, the electrical connectivity is maintained by interconnected cracked structures. (Figures S8 and S9, Supporting Information).

We also assessed the resistance stability at different temperatures (Figure 2e,f). During the first heat processing, a reduction of resistance with temperature up to 100 °C was observed, which we attribute to the thermal annealing of AgNWs and the resulting efficient contact of AgNWs at their junctions. In the second heating cycle, the resistance of both dual-sided nonwovens (PI/TPU/AgNW-500 and PI/TPU/AgNW-25) increased linearly with temperature increasing from room temperature to 160 °C, showing the metal-like behavior of electron transport as expected. The dual-sided nonwoven, PI/TPU/AgNW-500 even maintained a stable resistance for 1200 min at 250 °C (Figure 2g). PI/TPU/AgNW-500 also showed an excellent adhesion stability of AgNWs on PI nonwoven as seen in a washing test in soap water at 45 °C for 10 h in total (2 h for five times) (Figure 2h). PI/TPU/AgNW-500 maintained its low resistance after washing.

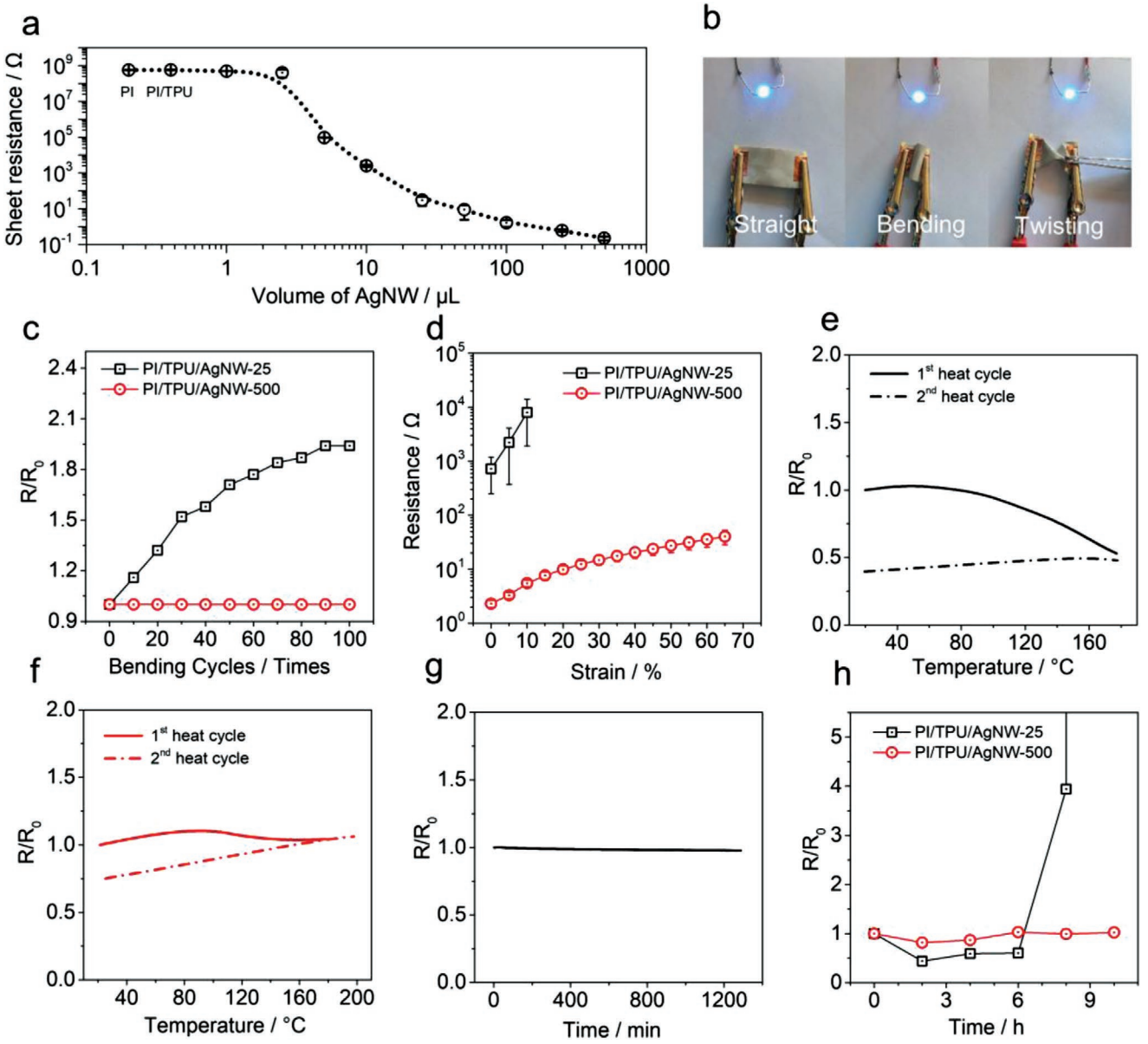

Figure 2. a) Sheet resistance of the dual-sided nonwovens prepared using different volumes of AgNW dispersion (17 g L^{-1}). PI and PI/TPU are labeled on the graphic without AgNWs for comparison. b) The luminance of LED bulb under different deformations of the dual-sided nonwoven. Resistance change of PI/TPU/AgNW-25 and PI/TPU/AgNW-500 on repeated c) bending cycles and d) different strain. e) The change of resistance of PI/TPU/AgNW-25 and f) PI/TPU/AgNW-500 upon temperature change. g) The change of resistance of PI/TPU/AgNW-500 at different time. h) The change of resistance of the dual-sided nonwoven after washing under different washing environments.

The PI/TPU/AgNW-500 demonstrated strong IR reflectance. The IR reflection performance of the samples was investigated by a setup, as depicted in **Figure 3**a and Figure S10, Supporting Information. The PI/TPU/AgNW-500 acts as a mirror in the mid IR range and, consequently, reflects thermal energy from a hot or cold source. This leads to a significant apparent temperature difference compared to PI (Figure 3b). Note that the exact determination of the absolute surface temperature of highly reflecting surfaces is very hard to conduct. We stress this fundamental issue in thermography by reporting an apparent temperature, which is merely a measure for the temperature of the surrounding environment than of the sample surface itself. The IR reflectance of the dual-sided nonwoven depends on the AgNW concentration (Figure 3c), whereas the reflectance of PI side is constant at ≈30%. We then characterized the optical properties of PI/TPU/AgNW-500 and pure PI electrospun nonwoven in more detail, including reflectance, absorptance, and transmittance spectra (Figure 3d,f). The PI/TPU/AgNW-500 show ultralow IR transmittance of 0.2% regardless of their orientation, which is expected to provide passive heating by hindering the thermal exchange between the human body and the ambient environment.[19] A very significant difference in absorptance and reflectance of the two sides of the nonwovens, AgNW side, and PI side, was observed. The dual-sided

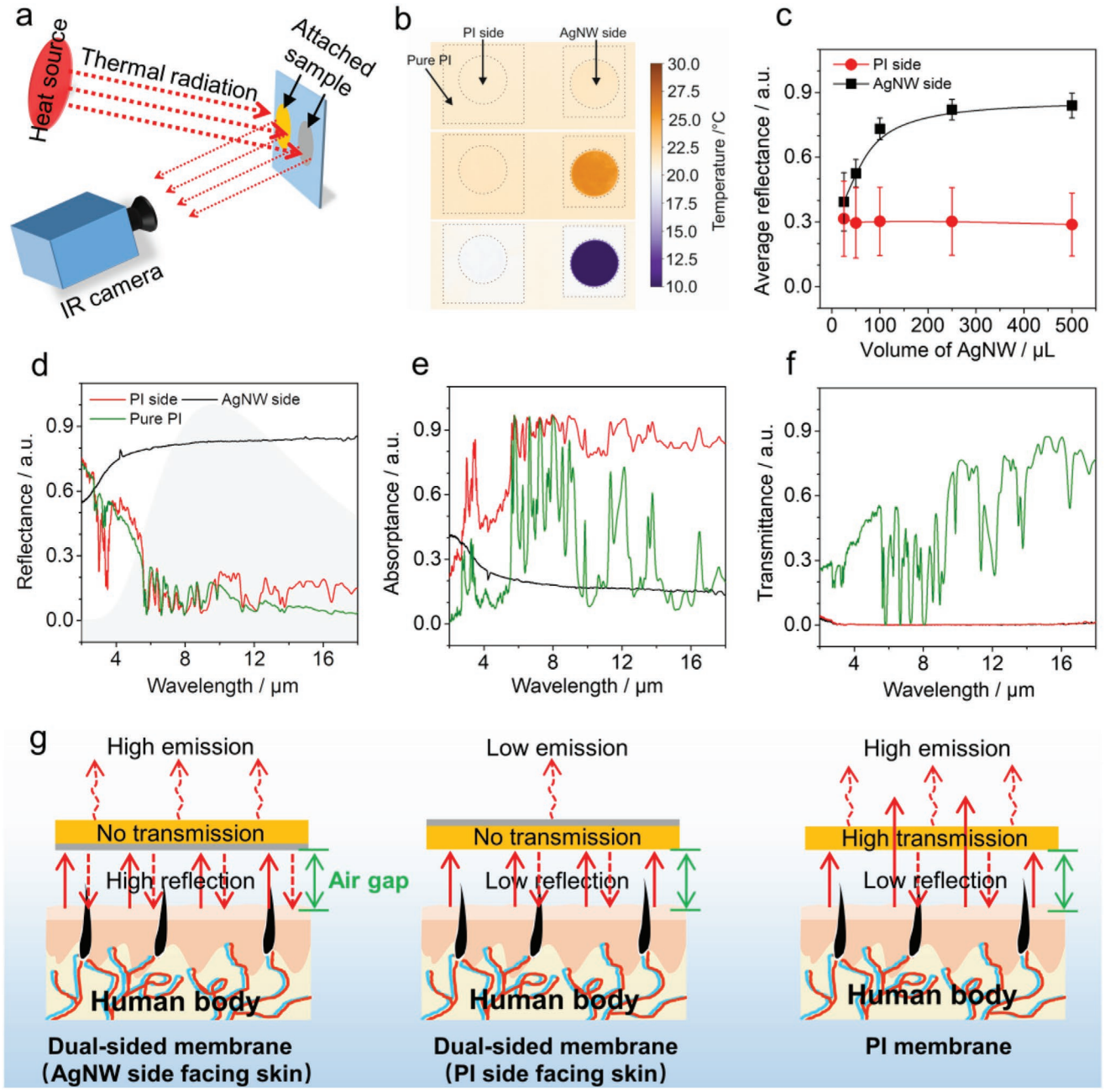

Figure 3. a) The schematic diagram of the setup for the measurement of IR reflection performance. b) Thermal images of IR reflection by dual-sided nonwoven (PI/TPU/AgNW-500). The AgNWs exhibited large apparent temperature difference compared to PI side. The first row: without hot/cold source; the second row: with hot source; the third row: with cold source. (Apparent temperature is defined as the temperature detected by IR camera without any correction) c) Average reflectance of a batch of dual-sided nonwovens with different amounts of AgNWs on the AgNW networks side and PI side. d) IR reflectance, e) absorptance, and f) transmittance of PI/TPU/AgNW-500 from another batch on the AgNW networks side and PI side. Gray area describes the major range of human body radiation. g) A schematic diagram of IR reflection by dual-sided nonwoven.

nonwoven exhibited low absorptance (19.5%) and high reflectance (80.3%) on the AgNWs side, and a high absorptance (78.5%) and low reflectance (21.1%) on the PI side. Compared to other AgNW coated textile, our nonwoven displayed a better IR reflection performance (Table S2, Supporting Information). We attribute this to the preparation procedure and the choice of AgNWs of appropriate length that allowed formation of flat and dense AgNW networks, reflecting most of IR irradiation as specular reflection and a minor portion as diffuse reflection. On the contrary, PI electrospun nonwovens (reflectance: 17.9%; absorptance: 30.6%; transmittance: 51.5%) and other polymeric materials, such as conventional textile, paper, and polystyrene foam, show poor IR reflectance.[20]

Continuous IR radiation loss from the human body into the ambient surroundings is the central reason for body heat loss. Materials with high emissivity have been demonstrated to dissipate more heat from objects to the ambient environment.[21] A textile for on-demand thermal management needs to maintain

the thermal comfort of the body in different environments, regulating temperature as required. The dual-sided nonwoven introduced here, can be worn in two orientations. This will change the mutual radiative energy exchange between skin, fabric, and environment, as the emittance strongly depends on the fabric orientation. According to Kirchhoff's law absorption equals emission. Furthermore, emittance E can be calculated by:

$$E = 1 - R - T \tag{1}$$

where R and T denote reflectance and transmittance, respectively. In the major range of human body radiation, a low emittance (≈20%) on the AgNW side was observed (Figure S11, Supporting Information). In contrast, the PI side presented a quite high emittance of >75% on an average. Figure 3g summarizes the different radiative contributions that will affect the entire system skin, fabric, and environment. One can expect that the AgNW layer will lead to less thermal losses, either since the energy exchange skin-nonwoven (AgNW facing skin) or nonwoven-environment (AgNW facing environment) will be reduced. The optimum orientation will, however, also be influenced by heat conduction at the bottom side and thermal convection at the top surface.

To judge the optimum orientation of the dual-sided nonwoven for a passive warming application, we designed an experiment that closely resembles all contributions (radiative, conductive, and convective) to the heat exchange in this multibody system. We characterize the overall heat loss of a pure PI electrospun nonwoven compared to PI/TPU/AgNW-500 with a setup as depicted in **Figure 4**a. A black coated copper plate resembles the high emission of skin and is set to a temperature of 35 °C. A small heater controlled and measured the required power until a steady-state temperature was reached as shown in Figure 4b. The nonwoven was loosely placed on the copper plate to mimic wearing of a textile. The surrounding dome acts as the ambient environment with a high emissivity/absorptivity at a temperature of ≈22 °C. The required power for the steady-state condition for the two orientations of the dual-sided nonwoven, the pure PI, and a graphite coated reference are displayed as a function of dome temperature (ambient) in Figure 4c. For both, pure PI samples and the PI side of the PI/TPU/AgNW-500 facing the dome more power is needed to maintain a skin temperature of 35 °C compared to the AgNW side facing outward. This indicates that the PI side losses more heat by radiative heat transfer to the environment than the AgNW side. This is in agreement with the collected optical data presented in Figure 3d–f. The pure PI electrospun nonwoven and the PI side of the PI/TPU/AgNW-500 show higher absorptance and are consequently expected to emit more radiation than the AgNW side (Figure 4d). The differences between pure PI and the PI side of PI/TPU/AgNW-500 in the mid IR range (>10 µm) have apparently no significant influence on the overall heat exchange. Furthermore, blocking of direct IR transmission by the AgNW layer facing towards the skin and a concomitant reduced radiative heat exchange between skin and fabric seems to have no measurable effect. The power consumption is the same for pure PI and the dual-sided nonwoven in this configuration. Consequently, for a contribution to passive warming only the dual-sided nonwoven with the AgNW facing to the outside will have an effect. Additionally, the PI electrospun nonwoven displayed a low thermal effusivity (88.1 W $s^{1/2}$ m^{-2} K^{-1}), which is comparatively low relative to other normal textiles (Figure 4e). Therefore, upon touching the skin the PI material will feel warm, suggesting that PI side facing towards skin (AgNW side facing towards outside) is the desirable wearing orientation.

A smart textile for thermal management needs to perform two functions: confining and providing heat to the human body for comfort. Thus, electric heating (active heating) usually is a popular and feasible way to offer extra thermal energy for warming a body. We, consequently, characterized the electrical heating performance of our dual-sided nonwovens by applying different direct currents. Electrical power (P) was distributed to the nonwoven by Joule heating according to Equation (2)

$$P = I^2 R \tag{2}$$

where I is applied current, and R is resistance. We used an IR camera to detect the apparent surface temperature of the sample after applying different electrical currents, which is illustrated in **Figure 5**a. The dual-sided nonwoven PI/TPU/AgNW-25 presented a rapid increase of the apparent surface temperature from room temperature to the equilibrium state within 5 s (Figure 5b and thermal images in Figure S12, Supporting Information). The apparent temperature could even go as high as 230 °C (Figure 5b) on increasing the current to 0.37 A. On the other hand, PI/TPU/AgNW-500 merely produced any Joule heat even at high direct current (DC) currents (0.37 A), exhibiting surface temperature close to room temperature. Note, that these apparent temperatures are not corrected to the low emissivity of the AgNW surface and, consequently, should only be taken for a relative estimation of the temperature changes upon electrical heating.

In order to take advantage of both active Joule heating and low radiation losses, we have integrated a nonwoven as a heating electrode (PI/TPU/AgNW-25) and another as a radiation insulator (PI/TPU/AgNW-500) in the form of a double layer (Figure S13, Supporting Information). PI/TPU/AgNW-25 and PI/TPU/AgNW-500 stacked together act as a thermal management device for heat compensation (Figure 5c). The PI side of the double layer was towards the skin. The apparent temperature of the palm was around 37 °C. The temperature profile of the as-designed thermal management device is provided in Figure 5d. Already by applying 0.1 A current the apparent temperature loss due to the low emissivity of the AgNW top layer is compensated. As expected, the apparent surface temperature increases even further with a higher DC current. This result indicates our thermal management device has a prominent heating function combining passive heating and active electric heating.

3. Conclusion

In conclusion, we have successfully prepared a breathable and flexible dual-sided nonwoven with tailored electrical and thermal properties that are promising as smart textiles for personal thermal management. The dual-sided nonwoven consisting of PI electrospun nonwoven and AgNW networks,

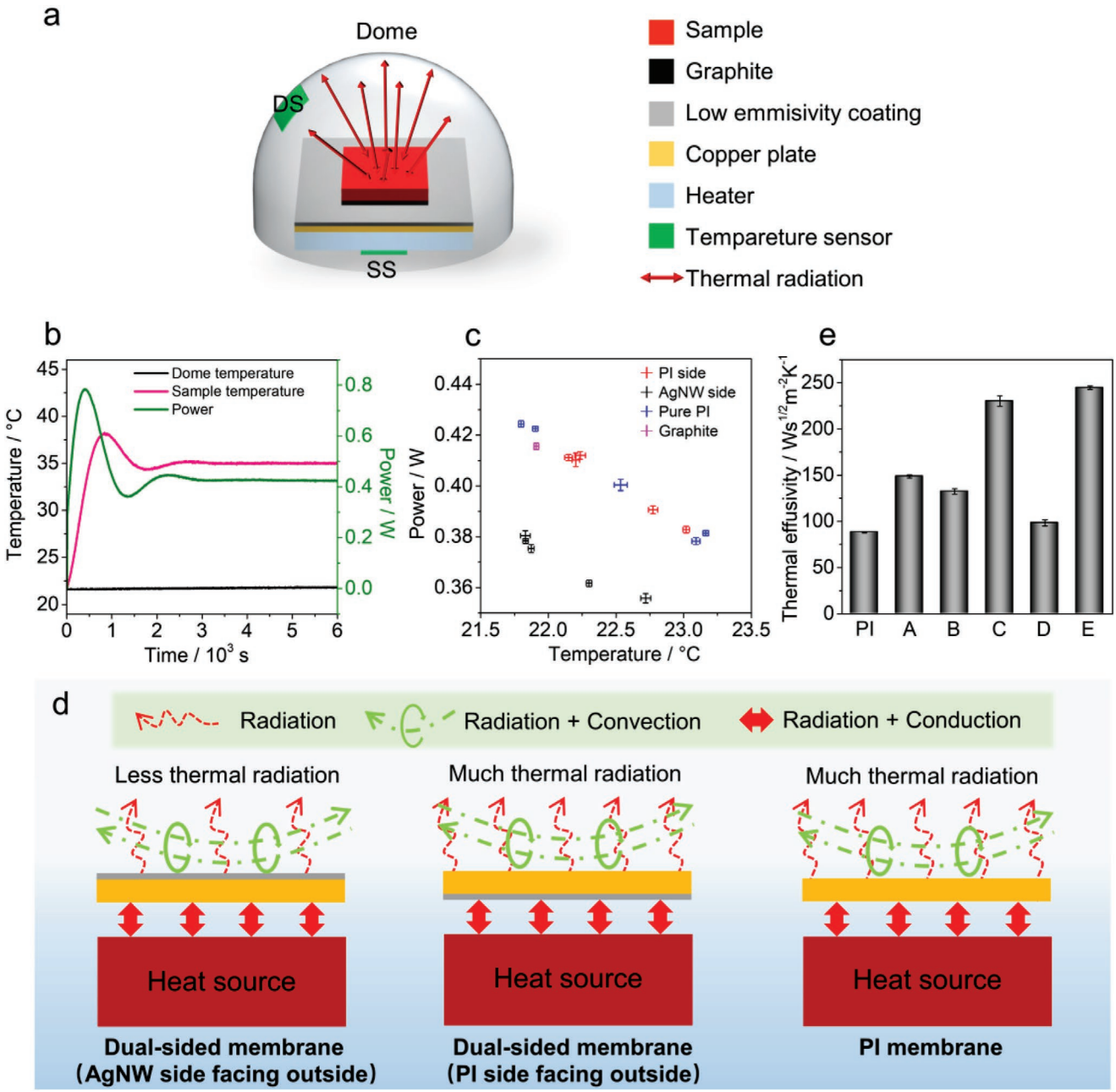

Figure 4. a) A schematic diagram of the setup for measuring radiatively dissipated energy. (SS: system sensor; DS: dome sensor) b) Evolution of dome temperature, sample temperature, and power supplied to the heater over time. c) Radiatively dissipated power for pure PI nonwoven, the respective sides of PI/TPU/AgNW-500, and a graphite reference as function of dome temperature (ambient). d) Schematic diagram of the thermal energy dissipation from PI/TPU/AgNW-500 and pure PI electrospun nonwoven. e) The effusivity of PI electrospun nonwoven and normal fabrics.[20] (PI: 35 layers of electrospun nonwoven, 10 g m^{-2} in each layer; A: 100% polyester, interlock knit fabric, 240 g m^{-2}; B: 100% polyester, interlock knit fabric, one side brushed, 255 g m^{-2}; C: 100% cotton, woven cotton duck fabric; D: 100% cotton, woven flannel fabric, 122 g m^{-2}; E: 100% cotton, woven poplin fabric, 180).

presented significant differences of physical, electrical, and thermal properties on the two sides, which could be tailored by using the amount of AgNW. More AgNW is prone to form dense AgNW networks, which possessed very low electrical resistance of 0.23 Ω sq^{-1} and excellent IR reflectance of more than 80%, far higher than the normal textiles. The dual-sided nonwoven with the AgNW facing to the outside demonstrated a desirable effect for a contribution to passive warming. It could be integrated into a thermal management device by applying low current, realizing both functions of reducing heat dissipation to the ambient environment and Joule heating to the human body. Besides, the dual-sided nonwoven showed outstanding flexibility under different deformations as well as washing stability without sacrificing electrical resistance. Such

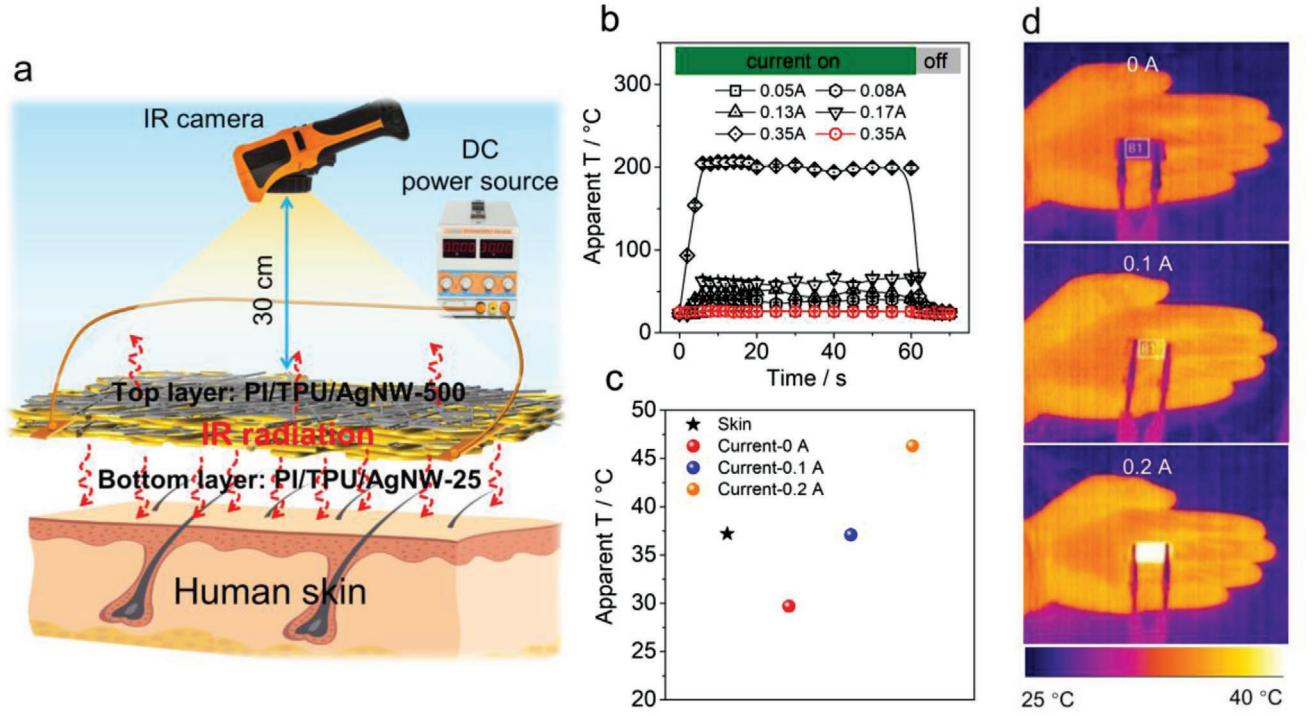

Figure 5. a) Schematic diagram of the smart textile for thermal management. The smart textile is composed of PI/TPU/AgNW-500 (top layer), to reduce thermal emissivity, and PI/TPU/AgNW-25 (bottom layer), to exhibit substantial Joule heating. b) Apparent surface temperature of PI/TPU/AgNW-25 heated by produced Joule heating with different current. (Black and red color represent PI/TPU/AgNW-25 and PI/TPU/AgNW-500 respectively.) c) Apparent surface temperature and d) corresponding thermal images of the thermal management device by the applied different current.

a dual-sided nonwoven can be used as a multifunctional flexible conductor and personal thermal management device to keep warm or smart textile escaping IR detection, which is very promising for next-generation wearable devices.

4. Experimental Section

Materials: PI electrospun nonwoven was kindly provided by Jiangxi Xiancai nanofiber Technology Co., Ltd. TPU (Desmopann DP 2590, Bayer Materials Science, Mn 88 900, Mw 145 000), ethylene glycol (p.a. ≥99.5%, Fluka), poly(vinylpyrrolidone) (PVP K30, Mw 40 000, Sigma-Aldrich), silver nitrate ($AgNO_3$, p.a. 99.9%, Sigma-Aldrich), iron chloride ($FeCl_3$, p.a. 98.0%, Sigma-Aldrich), sodium chloride (NaCl, p.a. 99.0%), tetrahydrofuran (THF, distilled) were used as obtained. Other solvents were distilled before use. The AgNWs were synthesized by a solvent thermal method.[14b,c]

The preparation of dual-sided nonwoven: A piece of PI electrospun nonwoven (5 cm × 5 cm) was placed on a sand core funnel, followed by filtering AgNW aqueous dispersion through the PI nonwoven under vacuum assistance to obtain the PI/AgNW network. The used amount of AgNW is shown in Table S1, Supporting Information. Next, the dual-sided nonwoven was fabricated by filtering a TPU solution (2 mL, 8 wt%, in THF) through the PI/AgNW network under light vacuum to physically bond AgNWs strongly onto the PI nonwoven. At last, the resulted sample was naturally dried in the fume hood for 24 h. The relevant parameters used during different steps are tabulated in Table S3, Supporting Information.

The scanning electron microscopy (SEM) (Zeiss LEO1530, Jena, Germany) was employed for observing PI nanofibers and AgNW networks. Energy-dispersive X-ray spectroscopy (EDX) was performed by using a Zeiss Ultra Plas (Jena, Germany; 10 kV acceleration voltage). Pore size distribution measurements were used to investigate pore size of the samples (Toper as standard test liquid with surface tension of 16.0 mN m^{-1}). The air permeability of the samples was measured by the Air Permeability Tester (FX 3300 LabAir IV, Switzerland) with the test area of 5 cm^2 under the pressure of 98 Pa. Each sample was measured five times at least, and the average value was taken. Tensile tester (Zwick/Roell BT1-FR 0.5TN-D14, Germany) was employed to characterize the mechanical property of samples. The samples (2 cm in length, 2 mm in width) were stretched at a speed of 10 mm min^{-1} (20 °C, pretension 0.01 N mm^{-1}). The thickness of samples was determined by a screw micrometer.

The washing test was performed by dipping the samples into 45 °C soap water (1 mL Manisoft detergent dissolved into 50 mL DI water) respectively with 100 rpm min^{-1} stirring for washing. The resistance of PI/TPU/AgNW-500 upon temperature and time was conducted with van der Pauw method. Sheet resistance was measured (Four-point measurements) with Keithley 2420 High-Current Source Meter coupled with Signatone SYS-301. Stretching resistance of different strain and cycling bending tests were performed by a tensile tester (Zwick/Roell BT1-FR 0.5TN-D14, Germany) to monitor stretching distance and bending degrees. An EMOS Multimeter (EM391) was connected by a copper conductor to detect the electrical resistance change of samples in different strain and bending cycles.

The IR reflection images were recorded by placing the samples in a cardbox enclosure. Images with a closed box and a hot or cold source above the camera were recorded (VarioCAM HD research 875/30 mm, Infratec) as shown in Figure 3a,b.

FTIR-spectroscopy measurements were conducted with an IR-spectrometer (Vertex 70, Bruker) in combination with a gold-coated integrating sphere accessory (A562, Bruker). The reflectance and transmittance were measured at the respective ports of the sphere. As reference a diffuse gold standard was used. The absorptance/emittance was calculated as Equation (1).

The radiative energy loss of the nonwoven was approximated with a steady-state heat transfer experiment. A circular sample piece with a

diameter of 3 mm was measured in a self-build setup. The sample was placed on a copper plate that was coated with graphite at the sample area and reflective aluminum foil at the outside, respectively. The copper plate was placed on a feedback-controlled heater and the power used to keep the sample at 35 °C (skin temperature) was recorded. The temperature sensor for the feedback control was in contact with the heater to record the sample temperature. The entire heater setup was placed within a block of expanded polystyrene to reduce heat losses by conduction to the surrounding. The heater block was placed below a graphite-coated aluminum dome with a diameter of 75 cm. The dome acts as a heat sink and was kept at ambient temperature during the experiment, which was monitored with a second temperature sensor. For a typical measurement, the sample was placed on the heater and the sample temperature, the dome temperature, and the heater power were monitored every 5 s until a steady state was reached. For each sample, the power and temperature data of 30 min in steady-state were averaged.

The thermal effusivity of the pure PI fabric was determined with a modified transient plane source instrument as described in the ASTM-D7984 standard.[22] Nonwoven pieces with a size of 5 × 5 cm are stacked to reach a sufficient overall thickness for the measurement. To eliminate the influence of any preferred orientation each layer was positioned with a rotation of 30° with respect to the previous layer. For the measurement, a thermal conductivity analyzer (TCi C-Therm, Canada) with a circular probe area of 1.75 cm^2 was used. During the measurement, a pressure of 10 N was applied to the stack to ensure good contact.

Different constant electrical currents of 0.05, 0.08, 0.13, 0.17, 0.35, and 0.37 A are applied by a DF-3010 DC power supply to investigate joule heating effect (1 cm × 3 cm, connected with copper cable). A TrueIR camera (Keysight U5856A) was employed to record the temperature of samples, and time-dependent joule heating was depicted by the Origin software.

The detailed preparation procedure of the thermal management device is shown in Figure S13, Supporting Information. The DF-3010 DC power supply was employed to provide constant currents. An IR camera was used to detected surface temperature as shown in Figure 5a.

Supporting Information

Supporting Information is available from the Wiley Online Library or from the author.

Acknowledgements

Q.G. would like to thank the China Scholarship Council for awarding a fellowship for carrying out Ph.D. research in Germany in the lab of Prof. Andreas Greiner. This project has received funding from the European Research Council (ERC) under the European Union's Horizon 2020 research and innovation program (grant agreement no. 714968) and by Deutsche Forschungsgemeinschaft (project no. 431073172). The authors further want to thank Qimeng Song for the help with the heat transfer experiment, Thomas Tran for support with the IR camera images and Ina Klein for the assistance with the thermal effusivity measurements. The authors also would like to acknowledge Bavarian Polymer Institute (BPI) for providing SEM instruments for sample characterizations.

Open access funding enabled and organized by Projekt DEAL.

Conflict of Interest

The authors declare no conflict of interest.

Data Availability Statement

The data that supports the findings of this study are available in the supplementary material of this article.

Keywords

electrospinning, heat management, Janus fabrics, thermal emission, wearable devices

Received: September 1, 2021
Revised: September 27, 2021
Published online:

[1] a) W. Weng, P. N. Chen, S. S. He, X. M. Sun, H. S. Peng, *Chem. Int. Ed.* **2016**, *55*, 6140; b) S. Liu, K. Ma, B. Yang, H. Li, X. Tao, *Adv. Funct. Mater.* **2021**, *31*, 2007254.

[2] a) X. Pu, W. X. Song, M. M. Liu, C. W. Sun, C. H. Du, C. Y. Jiang, X. Huang, D. C. Zou, W. G. Hu, Z. L. Wang, *Adv. Energy Mater.* **2016**, *6*, 1601048; b) C. Li, M. M. Islam, J. Moore, J. Sleppy, C. Morrison, K. Konstantinov, S. X. Dou, C. Renduchintala, J. Thomas, *Nat. Commun.* **2016**, *7*, 13319.

[3] Y. C. Peng, Y. Cui, *Joule* **2020**, *4*, 724.

[4] a) R. Hu, Y. D. Liu, S. Shin, S. Y. Huang, X. C. Ren, W. C. Shu, J. J. Cheng, G. M. Tao, W. L. Xu, R. K. Chen, X. B. Luo, *Adv. Energy Mater.* **2020**, *10*, 1903921; b) D. Y. Miao, X. F. Wang, J. Y. Yu, B. Ding, *Adv. Funct. Mater.* **2021**, *31*, 2008705.

[5] a) P. C. Hsu, A. Y. Song, P. B. Catrysse, C. Liu, Y. C. Peng, J. Xie, S. H. Fan, Y. Cui, *Science* **2016**, *353*, 1019; b) Y. C. Peng, J. Chen, A. Y. Song, P. B. Catrysse, P. C. Hsu, L. L. Cai, B. F. Liu, Y. Y. Zhu, G. M. Zhou, D. S. Wu, H. R. Lee, S. H. Fan, Y. Cui, *Nat. Sustain.* **2018**, 105.

[6] a) P. C. Hsu, C. Liu, A. Y. Song, Z. Zhang, Y. C. Peng, J. Xie, K. Liu, C. L. Wu, P. B. Catrysse, L. L. Cai, S. Zhai, A. Majumdar, S. H. Fan, Y. Cui, *Sci. Adv.* **2017**, *3*, 1700895; b) L. L. Cai, A. Y. Song, P. L. Wu, P. C. Hsu, Y. C. Peng, J. Chen, C. Liu, P. B. Catrysse, Y. Y. Liu, A. K. Yang, C. X. Zhou, C. Y. Zhou, S. H. Fan, Y. Cui, *Nat. Commun.* **2017**, *8*, 496.

[7] Y. Lu, X. D. Xiao, J. Fu, C. M. Huan, S. Qi, Y. J. Zhan, Y. Q. Zhu, G. Xu, *Chem. Eng. J.* **2019**, *355*, 532.

[8] Y. Cui, H. X. Gong, Y. J. Wang, D. W. Li, H. Bai, *Adv. Mater.* **2018**, *30*, 1706807.

[9] P. C. Hsu, X. G. Liu, C. Liu, X. Xie, H. R. Lee, A. J. Welch, T. Zhao, Y. Cui, *Nano Lett.* **2015**, *15*, 365.

[10] A. Hazarika, B. K. Deka, D. Kim, H. E. Jeong, Y. B. Park, H. W. Park, *Nano Lett.* **2018**, *18*, 6731.

[11] S. H. Jiang, J. Y. Cheong, J. S. Nam, I. D. Kim, S. Agarwal, A. Greiner, *ACS Appl. Mater. Interfaces* **2020**, *12*, 19006.

[12] a) F. Zhang, Y. Y. Feng, M. M. Qin, L. Gao, Z. Y. Li, F. L. Zhao, Z. X. Zhang, F. Lv, W. Feng, *Adv. Funct. Mater.* **2019**, *29*, 1901383; b) H. L. Li, S. C. Dai, J. Miao, X. Wu, N. Chandrasekharan, H. X. Qiu, J. H. Yang, *Carbon* **2018**, *126*, 319.

[13] Y. Wang, W. Wang, X. D. Ding, D. Yu, *Chem. Eng. J.* **2020**, *380*, 122553.

[14] a) S. H. Jiang, S. Reich, B. Uch, P. Hu, S. Agarwal, A. Greiner, *ACS Appl. Mater. Interfaces* **2017**, *9*, 34286; b) Q. Gao, B. A. F. Kopera, J. Zhu, X. J. Liao, C. Gao, M. Retsch, S. Agarwal, A. Greiner, *Adv. Funct. Mater.* **2020**, *30*, 1907555; c) S. Reich, M. Burgard, M. Langner, S. H. Jiang, X. Q. Wang, S. Agarwal, B. Ding, J. Y. Yu, A. Greiner, *npj Flexible Electron.* **2018**, *2*, 5.

[15] a) J. W. Lee, S. Jung, T. W. Lee, J. Jo, H. Y. Chae, K. Choi, J. J. Kim, J. H. Lee, C. Yang, J. M. Baik, *Adv. Energy Mater.* **2019**, *9*, 1901987; b) L. Dhakar, P. Pitchappa, F. E. H. Tay, C. Lee, *Nano Energy* **2016**, *19*, 532; c) J. Chen, Z. L. Wang, *Joule* **2017**, *1*, 480.

[16] a) F. C. Li, Y. Liu, X. L. Shi, H. P. Li, C. H. Wang, Q. Zhang, R. J. Ma, J. J. Liang, *Nano Lett.* **2020**, *20*, 6176; b) H. J. Kim, K. Sim, A. Thukral, C. J. Yu, *Sci. Adv.* **2017**, *3*, e1701114; c) J. Kim, M. Kim, M. S. Lee, K. Kim, S. Ji, Y. T. Kim, J. Park, K. Na, K. H. Bae, H. K. Kim, F. Bien, C. Y. Lee, J. U. Park, *Nat. Commun.* **2017**, *8*, 14997; d) S. S. Yao,

P. Ren, R. Q. Song, Y. X. Liu, Q. J. Huang, J. Y. Dong, B. T. O'Connor, Y. Zhu, *Adv. Mater.* **2020**, *32*, 1902343; e) J. K. Han, J. K. Yang, W. W. Gao, H. Bai, *Adv. Funct. Mater.* **2021**, *31*, 2010155.

[17] S. Cho, S. Kang, A. Pandya, R. Shanker, Z. Khan, Y. Lee, J. Park, S. L. Craig, H. Ko, *ACS Nano* **2017**, *11*, 4346.

[18] a) X. W. Liang, T. Zhao, W. Jiang, X. C. Yu, Y. G. Hu, P. L. Zhu, H. R. Zheng, R. Sun, C. P. Wong, *Nano Energy* **2019**, *59*, 508; b) F. Liang, X. J. Zhao, H. Y. Li, Y. J. Fan, J. W. Cao, Z. L. Wang, G. Zhu, *Nano Energy* **2020**, *69*, 104414; c) Z. Li, Q. Zheng, Z. L. Wang, Z. Li, *Research (Wash D C)* **2020**, *2020*, 8710686.

[19] a) L. L. Cai, A. Y. Song, W. Li, P. C. Hsu, D. C. Lin, P. B. Catrysse, Y. Y. Liu, Y. C. Peng, J. Chen, H. X. Wang, J. W. Xu, A. K. Yang, S. H. Fan, Y. Cui, *Adv. Mater.* **2018**, *30*, 1802152; b) X. A. Zhang, S. Yu, B. Xu, M. Li, Z. Peng, Y. Wang, S. Deng, X. Wu, Z. Wu, M. Ouyang, *Science* **2019**, *363*, 619.

[20] a) Y. Lian, H. Yu, M. Wang, X. Yang, Z. Li, F. Yang, Y. Wang, H. Tai, Y. Liao, J. Wu, *J. Mater. Chem. C* **2020**, *8*, 8399; b) X. Yue, T. Zhang, D. Yang, F. Qiu, Z. Li, G. Wei, Y. Qiao, *J. Colloid Interface Sci.* **2019**, *535*, 363.

[21] T. Li, Y. Zhai, S. M. He, W. T. Gan, Z. Y. Wei, M. Heidarinejad, D. Dalgo, R. Y. Mi, X. P. Zhao, J. W. Song, J. Q. Dai, C. J. Chen, A. Aili, A. Vellore, A. Martini, R. G. Yang, J. Srebric, X. B. Yin, L. B. Hu, *Science* **2019**, *364*, 760.

[22] ASTM D7984-16, *Standard Test Method for Measurement of Thermal Effusivity of Fabrics Using a Modified Transient Plane Source (MTPS) Instrument*, ASTM International, West Conshohocken, PA **2016**.